

On the design and characterisation of a microwave microstrip resonator for gas sensing applications

Giovanni Gugliandolo¹, Davide Aloisio², Giuseppe Campobello¹, Giovanni Crupi³, Nicola Donato¹

¹ Department of Engineering, University of Messina, Italy

² CNR ITAE, Messina, Italy

³ BIOMORF Department, University of Messina, Italy

ABSTRACT

This study focuses on the microwave characterisation of a microstrip resonator aimed for gas sensing applications. The developed one-port microstrip resonator, consisting of three concentric rings with a central disk, is coupled to a 50-Ω microstrip feedline through a small gap. A humidity sensing layer is deposited on this gap by drop-coating an aqueous solution of Ag@α-Fe₂O₃ nanocomposite. The operation principle of the developed humidity sensor is based on the change of the dielectric properties of the Ag@α-Fe₂O₃ nanocomposite when the relative humidity is varied. However, it should be underlined that, depending on the choice of the sensing material, different target gases of interest can be detected with the proposed structure. The frequency-dependent response of the sensor is obtained using the reflection coefficient measured from 3.5 GHz to 5.6 GHz, with relative humidity ranging from 0 %rh to 83 %rh. The variation of the humidity concentration strongly impacts on the two resonances detected in the measured reflection coefficient. In particular, an increase of the humidity level leads to lowering both resonant frequencies, which can be used as sensing parameters for humidity monitoring purpose. An exponential function has been used to accurately model the two resonant frequencies as a function of the humidity.

Section: RESEARCH PAPER

Keywords: Microwaves; resonators; gas sensors; metrological evaluation, humidity

Citation: Giovanni Gugliandolo, Davide Aloisio, Giuseppe Campobello, Giovanni Crupi, Nicola Donato, On the design and characterisation of a microwave microstrip resonator for gas sensing applications, Acta IMEKO, vol. 10, no. 2, article 9, June 2021, identifier: IMEKO-ACTA-10 (2021)-02-09

Section Editor: Ciro Spataro, University of Palermo, Italy

Received January 17, 2021; **In final form** May 4, 2021; **Published** June 2021

Copyright: This is an open-access article distributed under the terms of the Creative Commons Attribution 3.0 License, which permits unrestricted use, distribution, and reproduction in any medium, provided the original author and source are credited.

Corresponding author: Giovanni Gugliandolo, e-mail: giovanni.gugliandolo@unime.it

1. INTRODUCTION

Nowadays, the research interests in the development of sensors with extremely low-power consumption is growing because of the increasingly energy-saving requirements of the expanding market. This can be seen by the recent high demand of portable battery powered devices often used in wireless sensor networks (WSNs) for industrial (e.g., harmful gas detection) [1], [2], healthcare (e.g., wearable or implantable devices) [3]-[6], and environmental (e.g., weather forecast) [7]-[10] monitoring applications. Several sensor typologies have been investigated in order to achieve the best trade-off between performance and power consumption with a focus on size, weight, and production costs. In this context, microwave devices are considered as an attractive solution thanks to their interesting features in terms of cost, power consumption, and response time. They have been

employed for materials characterization [11]-[13] as well as for gas sensing applications [14].

Microwave gas sensors have the ability to operate at room temperature without the need of a heater [15], [16]. Moreover, they are fully compatible with wireless technology so that they can be easily integrated into wireless smart nodes [17]-[19]. In particular, the planar microstrip technology is widely employed in the fabrication of microwave components like antennas, filters, and resonators. Such devices are often used in sensing applications because of their low cost, easy fabrication, and good performance [20]-[24]. The microwave microstrip sensors are attractive especially for gas sensing applications, where the frequency-dependent dielectric properties of the sensing material are related with the adsorption of the target gas of interest on the sensing layer, deposited on the microstrip propagative structure. The progress in nanotechnologies has enabled advancements in the use of gas sensors using nanostructured materials as sensing layers [14], [25]-[27].

Following on from the results of our previous study [28], we present here a thorough investigation of a one-port gas transducer based on a microwave microstrip resonator, which is validated as humidity sensor by using an $\text{Ag}@\alpha\text{-Fe}_2\text{O}_3$ nanocomposite as a sensing material. The experimental-based investigation is performed by focusing the analysis on both magnitude and phase of the reflection coefficient (Γ) and its corresponding impedance (Z). In particular, we monitored the relative humidity over the broad range going from 0% to 83% at room temperature, and by assessing the sensing performance of the developed gas transducer to change in the relative humidity in terms of variations in the frequency-dependent behaviour of Γ . As shown later in this paper, two dips are clearly visible in the magnitude of Γ for the proposed sensor at approximately 3.7 GHz and 5.4 GHz, and their appearance is shifted towards lower frequencies when the humidity level is increased. Hence, the resonant frequencies (f_{R1} and f_{R2}) associated to the two dips observed in Γ can be directly used as humidity sensing parameters. To this end, a sensitivity-based investigation is developed in order to assess the sensing performance of the proposed microwave sensor for humidity monitoring application. The humidity-dependent variations in the two resonant frequencies are accurately modelled by using an exponential function.

This article is structured as follows. Section II is dedicated to the design of the microstrip resonator, which is based on using three concentric rings with a central disk. This choice was made after a careful analysis of the performance of different resonator topologies through computer simulations. Compared to the traditional ring configuration [29], [30], the proposed topology allows improvement in the quality (Q -) factor and, thus, in the detection process. Section III is devoted to the development of the humidity sensor, which is based on using an $\text{Ag}@\alpha\text{-Fe}_2\text{O}_3$ nanocomposite as sensing material. It is worth noting that the high porosity of the nanostructure allows enhancement of the interaction with water vapour, thereby leading to an improved humidity sensitivity. Section IV is focused on the description of the fitting of the measurements locally around the two observed resonances by using a Lorentzian function. Section V is dedicated to the description of the setup for frequency- and humidity-dependent characterization and to the presentation of the experimental results. Finally, the conclusions are drawn in the last section.

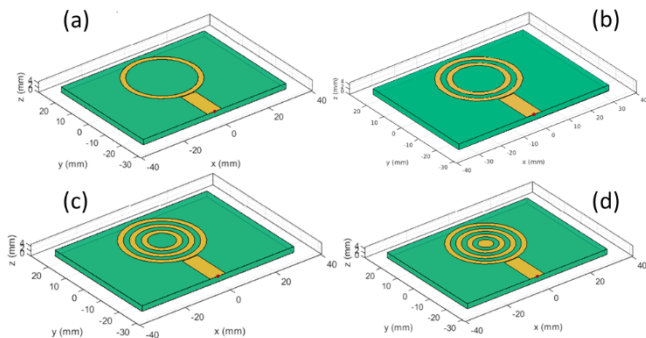


Figure 1. Illustration of the four studied resonator topologies: (a) traditional ring, (b) two concentric rings, (c) three concentric rings, and (d) three concentric copper rings with a central disk.

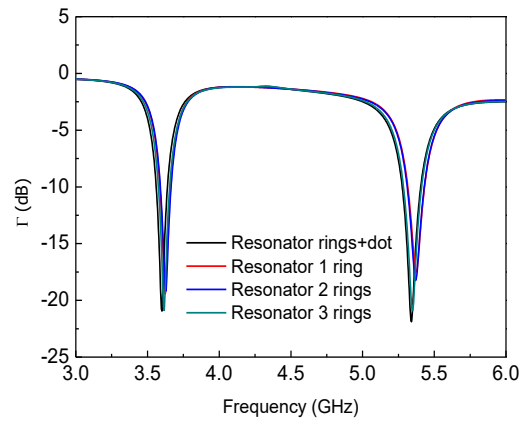


Figure 2. Behaviour of the magnitude of the simulated reflection coefficient versus frequency from 3.0 GHz to 6.0 GHz for the four studied resonator topologies.

2. RESONATOR DESIGN AND SIMULATION

The proposed gas transducer is based on a concentric rings microstrip (CRM) resonator acting as a propagative structure for the electromagnetic waves. This novel topology of propagative structure is composed by three concentric copper rings with a 6-mm copper central disk and a 50- Ω microstrip feedline coupled to the resonator through a 0.2-mm gap.

The Matlab Antenna Toolbox was used for the design process. As illustrated in Figure 1, four different resonator topologies were considered during the design step based on computer simulations over the frequency range going from 3 GHz to 6 GHz: the classic ring resonator, two concentric rings, three concentric rings, and three concentric rings with a disk in the middle. Starting from the traditional configuration, the coupling gap and the ring thickness were optimized in terms of Q -factor. Later, additional rings were included in the design considering a constant spacing. Figure 3 shows the frequency-dependent behaviour of the magnitude of the simulated Γ for the four studied topologies. As can be observed, the computer simulations show that all investigated topologies have two resonances appearing in Γ , which can be detected as two marked dips occurring at about 3.7 GHz (i.e., Dip 1) and 5.4 GHz (i.e., Dip 2), respectively. The two dips are more clearly visible in

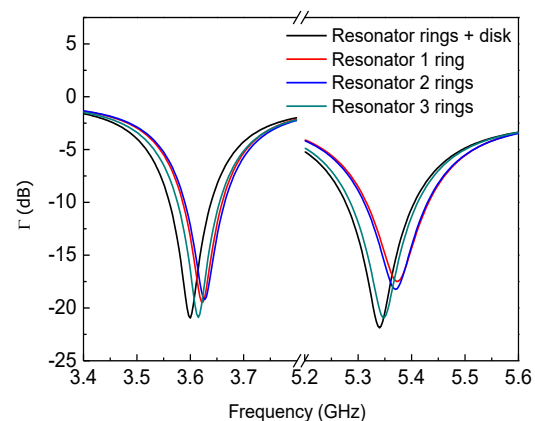


Figure 3. Illustration of the two dips appearing in the magnitude of the simulated reflection coefficient for the four studied resonator topologies.

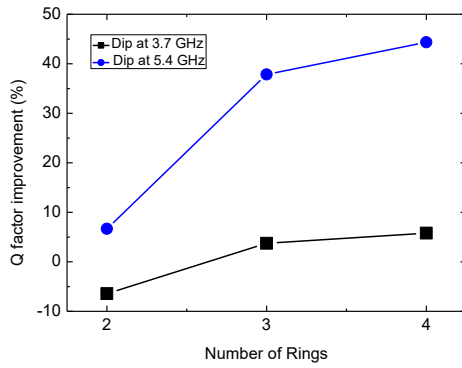


Figure 4. Analysis of the quality factor improvement of two resonances observed in the simulated reflection coefficient as a function of the number of rings of the resonator structure.

Figure 2, where the observation of Γ is limited to the two narrow frequency bands around f_{R1} and f_{R2} .

To assess the microwave performance of the studied resonator topologies, the quality factor improvement was evaluated by using the single-ring configuration as a reference for comparison. Figure 4 shows the Q -factor improvement for both resonances as a function of the number of concentric rings. It is worth noting that the selected topology (consisting of three rings with a central disk) allows achieving an improvement in the Q -factor equal to 6% and 44% at f_{R1} and f_{R2} , respectively.

The CRM resonator was fabricated on a 3.2-mm FR4 substrate [31] with copper as conductor for both top and ground layers by using the Protomat S103 PCB milling machine. The dielectric constant (ϵ_r) and the loss tangent ($\tan\delta$) of the substrate are 4.3 and 0.025, respectively. An SMA connector was soldered at the end of the 50- Ω microstrip feedline to connect the resonator with a vector network analyzer (VNA) for measuring Γ .

3. SENSOR DEVELOPMENT

To obtain the gas sensor, a sensing material was deposited on the surface of the propagative structure. In particular, an aqueous solution of $\text{Ag}@\alpha\text{-Fe}_2\text{O}_3$ nanocomposite was deposited on the gap placed between the external ring and the microstrip feedline by drop coating. The description and synthesis of this humidity sensing material is reported in [32]. The effect of the sensing material deposition on the frequency-dependent behaviour of Γ of the developed structure was measured from 3.5 GHz to 5.6 GHz using the Agilent 8753ES VNA with a one-port calibration (Short Open Load, Agilent 85052 mechanical calibration kit). As shown in Figure 5, both dips in Γ become much more pronounced after deposition, improving the quality factor of both dips. For the sake of completeness, the real and imaginary parts of the resonator input impedance for the selected frequency ranges are reported in Figure 6.

4. RESONATOR PARAMETERS EVALUATION

Estimating the resonant frequency (f_R), quality factor (Q), and dip amplitude (A_R) from a discrete frequency response is not a trivial task. A simple linear interpolation of the available discrete data can lead to an inaccurate estimation of these quantities, especially when the data are affected by noise. A better fitting approach consists in using a Lorentzian function [33], [34], which

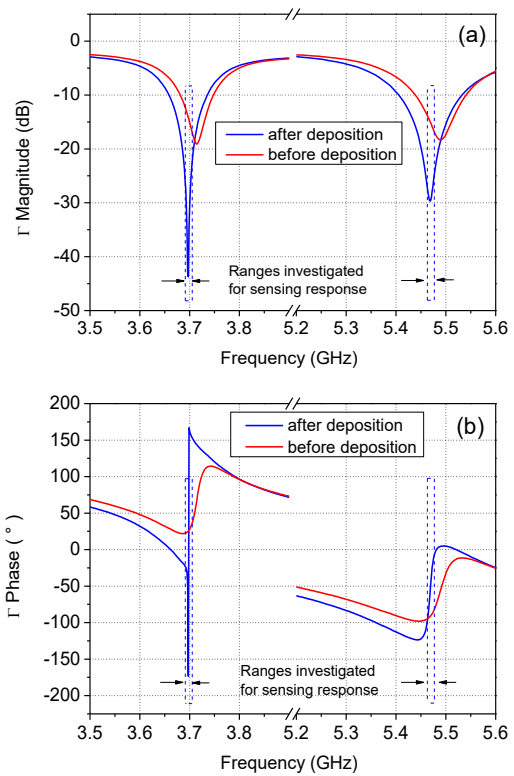


Figure 5. Behaviour of the (a) magnitude and (b) phase of the measured reflection coefficient as a function of frequency, from 3.5 GHz to 5.6 GHz, for the studied resonator before (red lines) and after (blue lines) deposition of the sensing material.

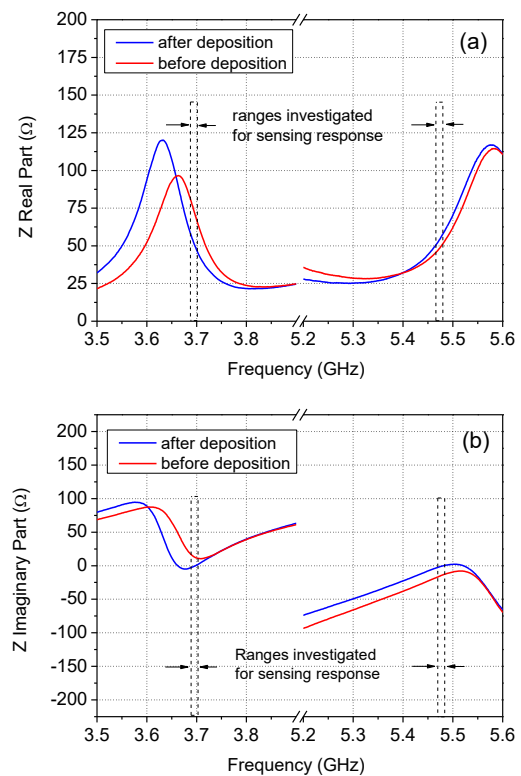


Figure 6. Behaviour of the (a) real and (b) imaginary parts of the impedance as a function of frequency from 3.5 GHz to 5.6 GHz, for the studied resonator before (red lines) and after (blue lines) deposition of the sensing material.

allows achieving a good estimation of the resonant parameters f_R , Q , and A_R . A more accurate result can be achieved by using a complex function to fit both real and imaginary parts of the spectrum [35], [36]. This technique can be useful in several applications in which the calibration procedure is impracticable (e.g., in cryogenic measurement systems) [36].

The frequency-dependent behaviour of the magnitude of Γ of the microwave resonator was modelled as a Lorentzian function:

$$|\Gamma(f)| = c_0 - \frac{a_0}{\pi} \cdot \frac{\frac{1}{2}G}{(f - f_R)^2 + \left(\frac{1}{2}G\right)^2}, \quad (1)$$

where f is the frequency, a_0 and a_0 are two real coefficients, and G is the full width at half maximum.

From equation (1), A_R and Q can be calculated respectively as:

$$A_R = c_0 - a_0 \cdot \frac{2}{\pi G}, \quad (2)$$

$$Q = \frac{f}{\Delta f} = \frac{f_R}{G\sqrt{\sqrt{2}-1}}, \quad (3)$$

where Δf is the resonator half-power bandwidth.

The Levenberg-Marquardt algorithm was used for fitting the measured data points with the Lorentzian function. It is found that the Lorentzian curve allows fitting very well the two observed resonant dips, so that it is possible to obtain a smooth behaviour of the magnitude of Γ over a continuous spectrum of frequencies for the estimation of the resonant parameters. As an illustrative example, Figure 7 reports the Lorentzian fitting applied to the magnitude of the measured Γ over a narrow frequency band around the second resonance. By using the fitting process, the parameters f_R , Q , and A_R can be accurately estimated over the whole considered humidity range.

5. EXPERIMENTAL RESULTS

The sensor was placed in a test chamber filled with a controlled atmosphere, where the electrical signal was supplied via an RF feed-through for connection with the Agilent 8753ES VNA (see Figure 8). The test chamber consists of a modified Petri dish made in Polystyrene, able to provide both a controlled atmosphere and good microwave propagation avoiding signal

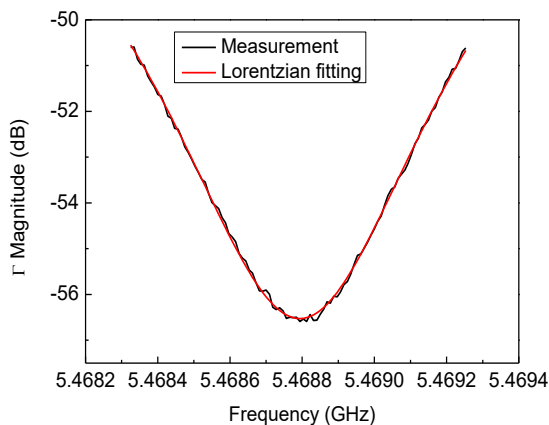


Figure 7. Illustration of the Lorentzian fitting (red line) of the magnitude of the measured (black line) reflection coefficient over a narrow frequency band around the second resonance for the studied resonator.

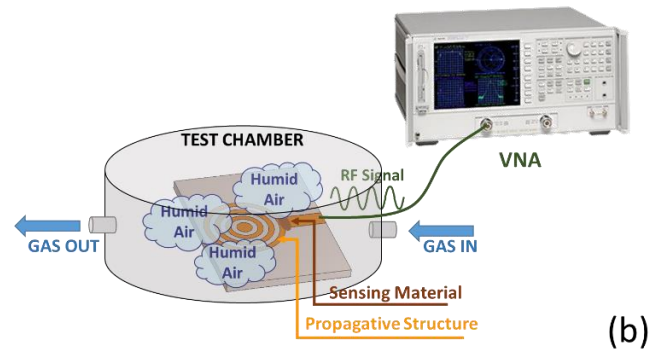
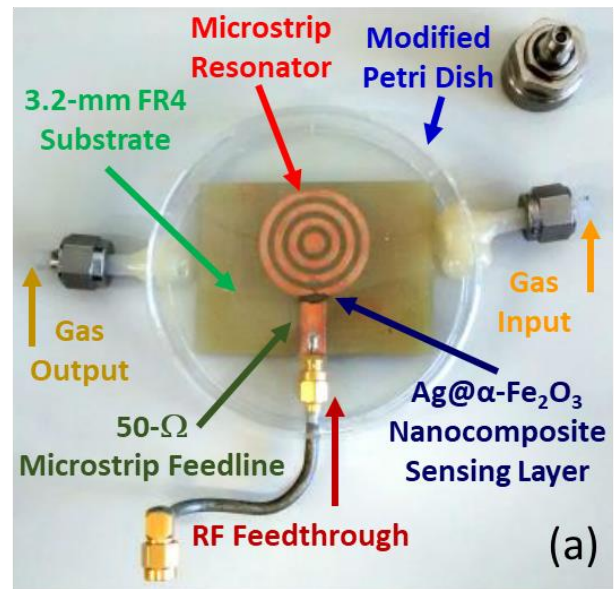


Figure 8. Illustration of (a) the sensor prototype placed in test chamber and (b) the frequency- and humidity-dependent characterization procedure.

perturbations. The developed sensor was characterized at seven different values of the relative humidity concentration, ranging from 0 %rh to 83 %rh, at room temperature. The 0 %rh nominal value was set by means of the certification of the gas bottles (0.5%).

The test gas mixture was set by means of a fully automated gas control system made by a certified gas bottle and a bubbler inside a thermostatic bath. The system is equipped with an array of Bronkhorst® mass flow controllers able to set a flux of 100 cm³/min in the test chamber, providing a fast set and purge for each test value of the humidity concentration.

The diagram of the gas apparatus is shown in Figure 9. After performing a one-port calibration, the reflection coefficient was measured at each humidity condition. Figure 10 and Figure 11 illustrate the impact of the relative humidity on the measured

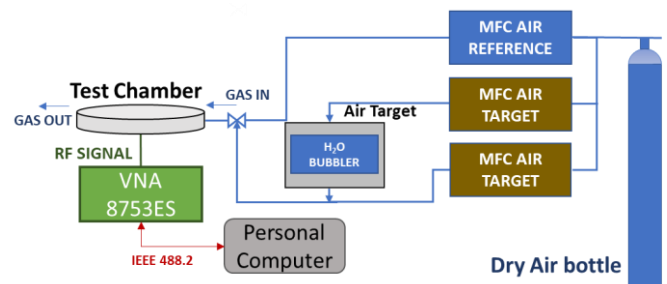


Figure 9. Illustration of the automated gas control and measurement system.

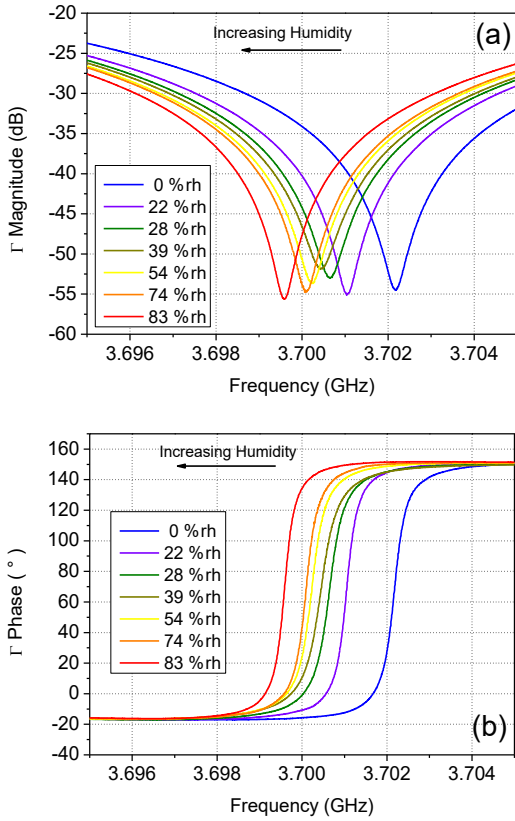


Figure 10. Behaviour of the (a) magnitude and (b) phase of the measured reflection coefficient over a narrow frequency band around the first resonance for the studied resonator, for seven relative humidity values.

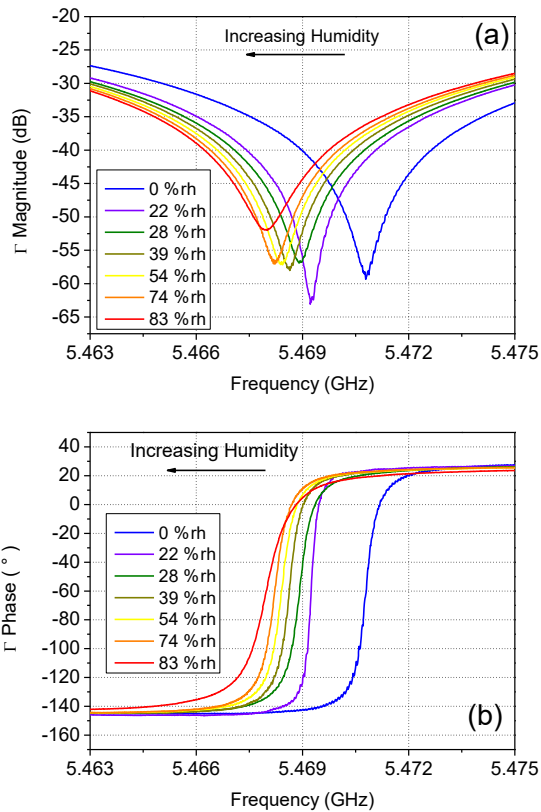


Figure 11. Behaviour of the (a) magnitude and (b) phase of the measured reflection coefficient over a narrow frequency band around the second resonance for the studied resonator at seven relative humidity values.

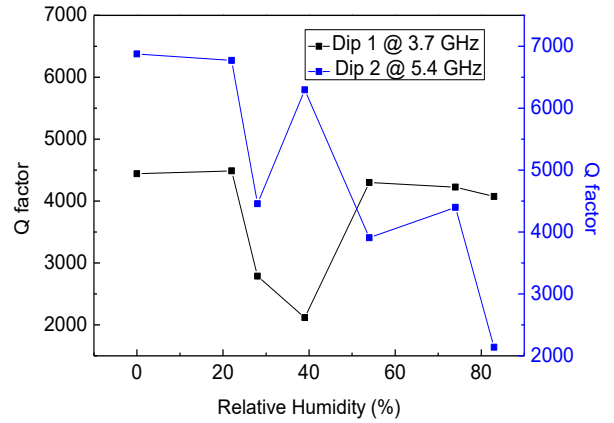


Figure 12. Analysis of the quality factor of two resonances observed in the measured reflection coefficient of the resonator as a function of the humidity.

behaviour of the complex reflection coefficient over two narrow frequency bands around the two observed dips, which were detected at approximately 3.7 GHz and 5.4 GHz. It can be seen that the size and the shape of the dips change significantly with the humidity values.

It should be mentioned that humidity-dependent variations are observed in all the three parameters f_R , Q -factor, and A_R for both resonances. Nevertheless, Q -factor and A_R do not follow a clear monotonic trend (see Figure 12 and Figure 13). On the other hand, it is worth noting that both resonant frequencies decrease with increasing the humidity level (see Figure 14), thereby enabling the use of the two resonant frequencies as humidity sensing parameters.

With the aim to evaluate the humidity sensing performance of the developed gas transducer for the whole investigated humidity range, we used an exponential function to fit the two resonant frequencies as a function of humidity:

$$f_R = A \cdot e^{\left(-\frac{RH}{B}\right)} + C, \quad (4)$$

where f_R represents the considered resonant frequency, RH is the relative humidity value, A , B , and C are the fitting parameters.

The calibration curve for both Dip 1 and Dip 2 is depicted in Figure 14(a); in Table 1 the fitting parameters are reported, while the calibration fit residuals are shown in Figure 14(b). For Dip 1

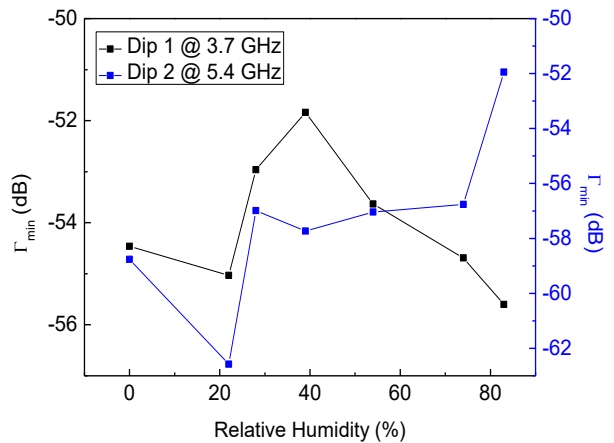


Figure 13. Magnitude of the measured reflection coefficient of the resonator at the first (black) and second (blue) resonances as a function of the humidity.

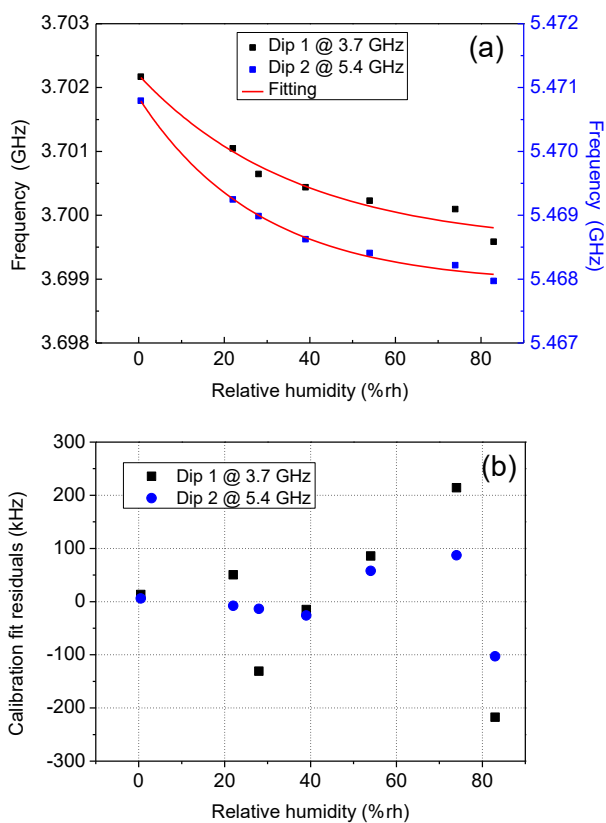


Figure 14. Calibration curve for both Dips (a) and calibration fit residuals (b).

residuals are almost within ± 200 kHz that, considering an absolute sensitivity of 26.4 kHz/%rh, corresponds to ± 7.6 %rh. On the other hand, Dip 2 exhibits a higher sensitivity (29.3 kHz/%rh) with lower calibration fit residuals in comparison to Dip 1: ± 100 kHz, or ± 3.4 %rh. As an alternative, it is possible to use both dips for humidity detection, thereby reducing the measurement error and increasing accuracy [37].

For the sake of completeness, the impact of the humidity variations is reported also for the impedance associated to the measured I , focusing on the two narrow frequency bands around the two dips. Figure 15 and Figure 16 show that a higher humidity implies that the real part decreases close to Dip 1 and then increases close to Dip 2, whereas the imaginary part is shifted towards higher values in both frequency bands.

6. CONCLUSIONS

A one-port microwave gas transducer was developed by coupling a microstrip resonator for electromagnetic wave propagation with an Ag@ α -Fe₂O₃ nanocomposite for humidity

Table 1. Fitting parameters values with standard errors for the two dips observed.

Parameter	Dip 1		Dip 2	
	Value	Standard error	Value	Standard error
A (MHz)	2.68	0.302	2.92	0.104
B (%rh)	37.21	10.349	28.18	2.485
C (MHz)	3699.51	0.3043	5467.92	0.088
	$R^2 = 0.994$		$R^2 = 0.956$	

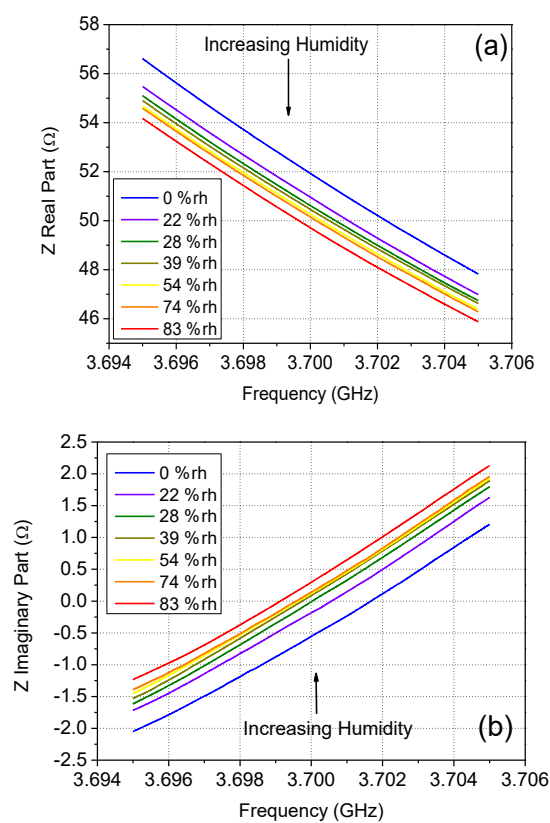


Figure 15. Behaviour of the (a) real and (b) imaginary parts of the measured impedance over a narrow frequency band around the first resonance for the studied resonator, for seven relative humidity values.

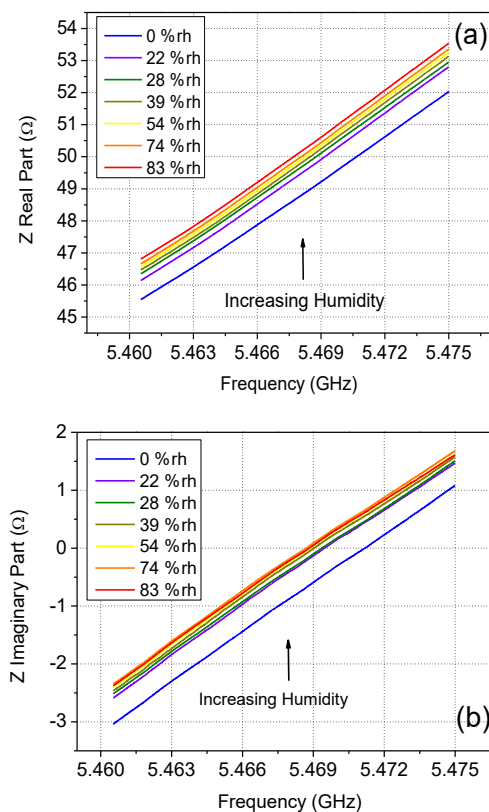


Figure 16. Behaviour of the (a) real and (b) imaginary parts of the measured impedance over a narrow frequency band around the second resonance for the studied resonator, for seven relative humidity values.

monitoring purpose. The sensing performance of this prototype was established by monitoring relative humidity from 0 %rh to 85 %rh at room temperature. To this end, the sensor was placed in a test chamber consisting of a modified Petri dish made in Polystyrene. By using a VNA, the reflection coefficient was measured over the 3.5 GHz ... 5.6 GHz frequency range, under seven different conditions of relative humidity. It was observed that the frequency-dependent behaviour of the reflection coefficient exhibits two marked dips that change in intensity, broadness, and location when the relative humidity is varied. In particular, the two detected resonant frequencies progressively shift towards lower values with increasing humidity, enabling their use as effective sensing parameters. The humidity-dependent behaviour of the two resonant frequencies was accurately reproduced by using an exponential function. The sensitivity-based analysis showed that the higher resonant frequency is the most sensitive parameter to change when the relative humidity is varied. Finally, it should be highlighted that, although the reported analysis was limited to the humidity sensing application, the developed transducer can be applied also for the detection of different target gases by selecting an appropriate sensing material tailored to the specific sensing application.

REFERENCES

- [1] P. C. Jain, R. Kushwaha, Wireless gas sensor network for detection and monitoring of harmful gases in utility areas and industries, 2012 Sixth International Conference on Sensing Technology (ICST), Kolkata, India, 18-21 Dec. 2012, pp. 642-646. DOI: [10.1109/ICSensT.2012.6461759](https://doi.org/10.1109/ICSensT.2012.6461759)
- [2] G. Campobello, M. Castano, A. Fucile, A. Segreto, WEVA: A complete solution for industrial internet of things, Lect. Notes in Computer Science, 10517 (2017) LNCS, pp. 231-238. DOI: [10.1007/978-3-319-67910-5_19](https://doi.org/10.1007/978-3-319-67910-5_19)
- [3] G. Campobello, A. Segreto, S. Zanafi, S. Serrano, An efficient lossless compression algorithm for electrocardiogram signals, 2018 26th European Signal Processing Conference (EUSIPCO), Rome, Italy, 3-7 Sept. 2018, pp. 777-781. DOI: [10.23919/EUSIPCO.2018.8553597](https://doi.org/10.23919/EUSIPCO.2018.8553597)
- [4] A. Darwish, A. E. Hassanien. Wearable and implantable wireless sensor network solutions for healthcare monitoring, Sensors 11(6) (2011), pp. 5561-5595. DOI: [10.3390/s110605561](https://doi.org/10.3390/s110605561)
- [5] X. Fu, W. Chen, Sh. Ye, Y. Tu, Y. Tang, D. Li, H. Chen, K. Jiang, A wireless implantable sensor network system for in vivo monitoring of physiological signals, IEEE Transactions on Information Technology in Biomedicine 15(4) (2011), pp. 577-584. DOI: [10.1109/TTTB.2011.2149536](https://doi.org/10.1109/TTTB.2011.2149536)
- [6] G. Gugliandolo, G. Campobello, P. Capra, S. Marino, A. Bramanti, G. Lorenzo, N. Donato, A movement-tremors recorder for patients of neurodegenerative diseases, IEEE Transactions on Instrumentation and Measurement 68(5) (2019), pp. 1451-1457. DOI: [10.1109/TIM.2019.2900141](https://doi.org/10.1109/TIM.2019.2900141)
- [7] F. Kiani, A. Seyyedabbasi, Wireless sensor network and internet of things in precision agriculture, International Journal of Advanced Computer Science and Applications 9(6) (2018). DOI: [10.14569/IJACSA.2018.090614](https://doi.org/10.14569/IJACSA.2018.090614)
- [8] G. Campobello, A. Segreto, S. Zanafi, S. Serrano, RAKE: A simple and efficient lossless compression algorithm for the Internet of Things 2017 25th European Signal Processing Conference (EUSIPCO), Kos, Greece, 28 August-2 September 2017, pp. 2581-2585. DOI: [10.23919/EUSIPCO.2017.8081677](https://doi.org/10.23919/EUSIPCO.2017.8081677)
- [9] S. Ullo, M. Gallo, G. Palmieri, P. Amenta, M. Russo, G. Romano, M. Ferrucci, A. Ferrara, M. De Angelis, Application of wireless sensor networks to environmental monitoring for sustainable mobility, 2018 IEEE International Conference on Environmental Engineering (EE), Milan, Italy, 12-14 March 2018, pp. 1-7. DOI: [10.1109/EE1.2018.8385263](https://doi.org/10.1109/EE1.2018.8385263)
- [10] G. Borrello, E. Salvato, G. Gugliandolo, Z. Marinkovic, N. Donato, UDOO-based environmental monitoring system. In: De Gloria A. (eds) Applications in Electronics Pervading Industry, Environment and Society. ApplePies, Lecture Notes in Electrical Engineering, 409 (2017) Springer, Cham. DOI: [10.1007/978-3-319-47913-2_21](https://doi.org/10.1007/978-3-319-47913-2_21)
- [11] P. Österberg, M. Heinonen, M. Ojanen-Saloranta, A. Mäkynen, Comparison of the performance of a microwave-based and an NMR-based biomaterial moisture measurement instrument, Acta IMEKO 5(4) (2016), pp. 88-99. DOI: [10.21014/acta_imeko.v5i4.391](https://doi.org/10.21014/acta_imeko.v5i4.391)
- [12] M. Scheffler, M. M. Felger, M. Thiemann, D. Hafner, K. Schlegel, M. Dressel, K. Ilin, M. Siegel, S. Seiro, C. Geibel, F. Steglich, Broadband Corbino spectroscopy and stripline resonators to study the microwave properties of superconductors, Acta IMEKO 4(3) (2015), pp. 47-52. DOI: [10.21014/acta_imeko.v4i3.247](https://doi.org/10.21014/acta_imeko.v4i3.247)
- [13] A. Alimenti, K. Torokhtii, N. Pompeo, E. Piuze, E. Silva, Characterisation of dielectric 3D-printing materials at microwave frequencies, Acta IMEKO 9(3) (2020), pp. 26-32. DOI: [10.21014/acta_imeko.v9i3.778](https://doi.org/10.21014/acta_imeko.v9i3.778)
- [14] G. Gugliandolo, D. Aloisio, S. G. Leonardi, G. Campobello, N. Donato, Resonant devices and gas sensing: from low frequencies to microwave range, Proc. of 14th Int. Conf. TELSIKS 2019, 23-25 October 2019, Nis, Serbia, Article n. 9002368, pp. 21-28. DOI: [10.1109/TELSIKS46999.2019.9002368](https://doi.org/10.1109/TELSIKS46999.2019.9002368)
- [15] T. Guo, T. Zhou, Q. Tan, Q. Guo, F. Lu, J. Xiong, A room-temperature CNT/Fe3O4 based passive wireless gas sensor, Sensors 18(10) (2018), art 3542. DOI: [10.3390/s18103542](https://doi.org/10.3390/s18103542)
- [16] K. Staszek, A. Szkudlarek, M. Kawa, A. Rydosz, Microwave system with sensor utilizing GO-based gas-sensitive layer and its application to acetone detection, Sensors and Actuators B: Chemical, 297 (2019), art. 126699. DOI: [10.1016/j.snb.2019.126699](https://doi.org/10.1016/j.snb.2019.126699)
- [17] B. Wu, X. Zhang, B. Huang, Y. Zhao, C. Cheng, H. Chen, High-performance wireless ammonia gas sensors based on reduced graphene oxide and nano-silver ink hybrid material loaded on a patch antenna, Sensors 17(9) (2017), art. 2070. DOI: [10.3390/s17092070](https://doi.org/10.3390/s17092070)
- [18] G. Gugliandolo, K. Naishadham, N. Donato, G. Neri, V. Fericola, Sensor-integrated aperture coupled patch antenna, 2019 IEEE International Symposium on Measurements & Networking (M&N), Catania, Italy, 8-10 July 2019, pp. 1-5. DOI: [10.1109/IWMN.2019.8805023](https://doi.org/10.1109/IWMN.2019.8805023)
- [19] G. Gugliandolo, K. Naishadham, G. Neri, V. C. Fericola, N. Donato, A novel sensor-integrated aperture Coupled microwave patch resonator for humidity detection, in IEEE Transactions on Instrumentation and Measurement 70 (2021), pp. 1-11. DOI: [10.1109/TIM.2021.3062191](https://doi.org/10.1109/TIM.2021.3062191)
- [20] G. Barochi, J. Rossignol, M. Bouvet, Development of microwave gas sensors, Sensors and Actuators B, 157(2) (2011), pp. 374-379. DOI: [10.1016/j.snb.2011.04.059](https://doi.org/10.1016/j.snb.2011.04.059)
- [21] M. H. Zarifi, T. Thundat, M. Daneshmand, High resolution microstrip resonator for sensing applications, Sensors and Actuators A: Physical 233 (2015), pp. 224-230. DOI: [10.1016/j.sna.2015.06.031](https://doi.org/10.1016/j.sna.2015.06.031)
- [22] D. Aloisio, N. Donato, Development of gas sensors on microstrip disk resonators, Procedia Engineering 87 (2014), pp. 1083-1086. DOI: [10.1016/j.proeng.2014.11.351](https://doi.org/10.1016/j.proeng.2014.11.351)
- [23] Z. Marinković, G. Gugliandolo, M. Latino, G. Campobello, G. Crupi, N. Donato, Characterization and neural modeling of a microwave gas sensor for oxygen detection aimed at healthcare applications, Sensors 20(24) (2020), art. 7150. DOI: [10.3390/s20247150](https://doi.org/10.3390/s20247150)

- [24] G. Gugliandolo, M. Latino, G. Campobello, Z. Marinkovic, G. Crupi, N. Donato, On the gas sensing properties of microwave transducers, 2020 55th International Scientific Conference on Information, Communication and Energy Systems and Technologies (ICEST), Niš, Serbia, 10-12 Sept. 2020, pp. 161-194. DOI: [10.1109/ICEST49890.2020.9232765](https://doi.org/10.1109/ICEST49890.2020.9232765)
- [25] S. B. Tooski, Sense toxins/sewage gases by chemically and biologically functionalized single-walled carbon nanotube sensor based microwave resonator, *J. Appl. Phys.* 107 (2010), art. 014702. DOI: [10.1063/1.3277020](https://doi.org/10.1063/1.3277020)
- [26] J. Park, T. Kang, B. Kim, et al., Real-time humidity sensor based on microwave resonator coupled with PEDOT:PSS conducting polymer film, *Scientific Reports* 8 (2018), art. 439. DOI: [10.1038/s41598-017-18979-3](https://doi.org/10.1038/s41598-017-18979-3)
- [27] A. Bogner, C. Steiner, S. Walter, J. Kita, G. Hagen, R. Moos, Planar microstrip ring resonators for microwave-based gas sensing: design aspects and initial transducers for humidity and ammonia sensing, *Sensors* 17(10) (2017), art. 2422. DOI: [10.3390/s17102422](https://doi.org/10.3390/s17102422)
- [28] G. Gugliandolo, D. Aloisio, G. Campobello, G. Crupi, N. Donato, Development and metrological evaluation of a microstrip resonator for gas sensing applications, *Proceedings of 24th IMEKO TC4 International Symposium and 22nd International Workshop on ADC and DAC Modelling and Testing, 2020*, pp. 80-84. Online [Accessed 14 June 2021] <https://www.imeko.org/publications/tc4-2020/IMEKO-TC4-2020-16.pdf>
- [29] M. T. Jilani, W. P. Wen, L. Y. Cheong, M. A. Zakariya, M. Z. U. Rehman, Equivalent circuit modeling of the dielectric loaded microwave biosensor, *Radioengineering* 23(4) (2014), pp. 1038-1047. Online [Accessed 14 June 2021] https://www.radioeng.cz/fulltexts/2014/14_04_1038_1047.pdf
- [30] D. L. K. Eng, B. C. Olbricht, S. Shi, D. W. Prather, Dielectric characterization of thin films using microstrip ring resonators, *Microwave and Optical Technology Letters* 57(10) (2015), pp. 2306-2310. DOI: [10.1002/mop.29321](https://doi.org/10.1002/mop.29321)
- [31] J. R. Aguilar, M. Beadle, P. T. Thompson, M. W. Shelley, The microwave and RF characteristics of FR4 substrates, *IEE Colloquium on Low Cost Antenna Technology (Ref. No. 1998/206)*, 1998, pp. 2/1-2/6. DOI: [10.1049/ic:19980078](https://doi.org/10.1049/ic:19980078)
- [32] A. Mirzaei, K. Janghorban, B. Hashemi, A. Bonavita, M. Bonyani, S. G. Leonardi, G. Neri, Synthesis, characterization and gas sensing properties of Ag@-Fe₂O₃ core-shell nanocomposites, *Nanomaterials* 5(2) (2015), pp. 737-749. DOI: [10.3390/nano5020737](https://doi.org/10.3390/nano5020737)
- [33] P. J. Petersan, S. M. Anlage, Measurement of resonant frequency and quality factor of microwave resonators: comparison of methods, *Journal of Applied Physics* 84(6) (1998). DOI: [10.1063/1.368498](https://doi.org/10.1063/1.368498)
- [34] M. P. Robinson, J. Clegg, Improved determination of Q-factor and resonant frequency by a quadratic curve-fitting method, *IEEE Trans. on Electrom. Comp.* 47(2) (2005), pp. 399-402. DOI: [10.1109/TEMC.2005.847411](https://doi.org/10.1109/TEMC.2005.847411)
- [35] G. Gugliandolo, S. Tabandeh, L. Rosso, D. Smorgon, V. Fericola, Whispering gallery mode resonators for precision temperature metrology applications, *Sensors* 21(8) (2021), art. 2844. DOI: [10.3390/s21082844](https://doi.org/10.3390/s21082844)
- [36] K. Torokhtii, A. Alimenti, N. Pompeo, E. Silva, Estimation of microwave resonant measurement uncertainty from uncalibrated data, *Acta IMEKO* 9(3) (2020), pp. 47-52. DOI: [10.21014/ACTA_IMEKO.V9I3.782](https://doi.org/10.21014/ACTA_IMEKO.V9I3.782)
- [37] S. Kiani, P. Rezaei, M. Navaei, Dual-sensing and dual-frequency microwave SRR sensor for liquid samples permittivity detection, *Measurement* 160 (2020), art. 107805. DOI: [10.1016/j.measurement.2020.107805](https://doi.org/10.1016/j.measurement.2020.107805)